APS physics

CHORUS

This is the accepted manuscript made available via CHORUS. The article has been published as:

Total X-Ray Scattering of Spider Dragline Silk

C. J. Benmore, T. Izdebski, and J. L. Yarger

Phys. Rev. Lett. **108**, 178102 — Published 24 April 2012

DOI: 10.1103/PhysRevLett.108.178102

Total X-Ray Scattering of Spider Dragline Silk

C.J. Benmore[1,3], T. Izdebski[2] and J.L. Yarger[*2,3]

(1) X-ray Science Division, Advanced Photon Source, Argonne National Laboratory, 9700 S. Cass Ave, IL 60439, U.S.A.

(2) Arizona State University, Department of Chemistry & Biochemistry, Tempe, AZ 85287-1604, USA.

(3) Arizona State University, Department of Physics, Tempe, AZ 85287, USA.

* Corresponding Author, jyarger@gmail.com

Abstract : Total x-ray scattering measurements of spider dragline silk fibers from *Nephila clavipes*, *Argiope aurantia* and *Latrodectus hesperus* all yield similar structure factors, with only small variations between the different species. X-ray scattering from fibers orientated perpendicular to the beam show a high degree of anisotropy and differential pair distribution functions (PDF) obtained by integrating over wedges of the equatorial and meridian planes indicate that, on average, the majority (95%) of the atom-atom correlations do not extend beyond 1 nm. Futhermore, the longest atom-atom correlations (at distances >2 nm) are not associated with the intense diffraction peaks at the lowest Q-values. Disordered molecular orientations along the fiber axis are consistent with proteins in similar structural arrangements to those in the equatorial plane, which may be associated with the silks greater flexibility in this direction.

Spider dragline silks are considered to be orientated fibers comprising of a small amount of crystalline material embedded in an amorphous matrix.[1-4] The generally accepted model structure of spider silk comprises of orientated nanocrystalline β-sheets joined by flexible amorphous strands.[5] Grubb and Jelinski[6] have suggested that the amorphous diffraction component in dragline silk is divided 60:40 between an isotropic ring and an orientated halo. The Scherrer equation[7] is commonly used to extract the coherence length from x-ray diffraction patterns of spider silks.[8-10] The coherence length provides an *estimate* of crystallite size and shape, by deconvoluting the low-Q features in the x-ray spectra into three sharp (crystalline) peaks plus a broad amorphous background. It has been proposed that the crystalline structure within spider dragline silk is comprised of hydrogen bonded β-sheets close in structure of poly-alanine[6] and the crystallite size along the *a, b* and *c* directions has been found to be approximately 5, 2 and 7 nm, respectively.[6, 10] However, strong overlap between the broad crystalline reflections and the orientated amorphous material makes extracting the peak full width half maximum (FWHM) problematic. Using crystalline and diffuse scattering proposed by W. Ruland[11], one can determine the degree of crystallinity of spider silks. By integrating the corrected intensity, provided the composition is known, values of 10-15% crystallinity have been obtained for *Nephila* dragline silk, the most studied species of spider silk.[6] However, this analysis must be performed over a wide Q-range and is not strictly valid when the disorder effects are strongly anisotropic, as in the case of spider dragline silks. Although much attention has been paid to the crystalline component of the silk, very few studies have investigated the structure of the larger amorphous component.[12]

In this work, we apply the method of total x-ray scattering[13], commonly used in the analysis of glassy and nano-crystalline materials to characterize the atomic structure of three different species of spider dragline silk, namely *Nephila clavipes*, *Argiope aurantia* and *Latrodectus hesperus*. X-ray and neutron total scattering techniques provide simultaneous information about long-range and short range ordering,[14] through the measurement of both Bragg peaks and diffuse scattering over a wide momentum transfer range. The Fourier transform of the structure factor S(Q) gives a real space pair distribution function. Although the instrumental resolution dictates the decay of the intensity at higher-r values, ordered crystalline peaks have been shown to persist up to a few hundred Angstrom in the pair distribution function (PDF).[13, 15] This type of analysis has therefore been successful in identifying the size of nano-particles in many different types of materials.[15-17] In this study, we use PDF methods to elucidate the atom-atom correlations and have found that the longest range ordering is *not* associated with the intense Bragg peaks at the lowest Q-values and that 95% of the correlations do not extend beyond 1 nm.

Wide-angle high-energy x-ray experiments[18] were performed on bundles of aligned fibers of *Nephila clavipes*, *Argiope aurantia* and *Latrodectus hesperus* dragline spider silks as a function of fiber orientation along and perpendicular to the direction of the x-ray beam. The fibers perpendicular to the x-ray beam were wound around washers with no extension of the fibers. The same bundle of fibers orientated along the beam axis, were held in 2 mm diameter polyimide tubes and cut to 3 mm in length. The measurements were performed on beamline 11-ID-C at the Advanced Photon Source

(APS) using an incident energy of 115 keV. The scattered intensity was measured over a Q-range of 0.4 to 14.2 $Å^{-1}$ using a *Mar345* image plate detector and over the range 0.4 to 19.3 $Å^{-1}$ using a *Perkin Elmer* a-Si flat panel detector during different experimental periods. Good agreement on the same silks was obtained during the different experimental runs. At this energy, the combination of very low absorption and low-flux (10^{11} photons/sec) leads to low dose rates and negligible radiation damage. Measurements at each orientation were typically taken with total count times of 10-20 minutes, and even after several hours exposure, no signs of radiation damage were observed in the scattered signal.

The 2D data were analyzed using the standard programs *FIT2D*[19] and *PDFgetX2*[20], correcting for background, beam polarization, Compton scattering, sample absortion, oblique incidence and detector efficiency. The data were divided into equatorial (60^{o} wedges, see figure 1) and meridional (120^{o} wedges), to highlight the anisotropic structural changes, and give adequate statistics at high-Q. The equatorial wedges were further subdivided into regions I and II and the meridional wedge into regions II, IV and V to investigate the influence of individual Bragg peaks on the pair distribution function. The elemental composition of each of the species of spider silks was measured using standard Amino Acid Analysis (AAA) and found to be $C_{24}H_{52}N_8O_{16}$ for all the fibers studied (to within atomic 5%).[21] The resulting Faber-Ziman x-ray structure factors S(Q) from the wedges are shown in figure 2(a). The diffraction patterns obtained for the silk fibers orientated perpendicular to the x-ray beam are similar for all species, the *Nephila clavipes* and *Argiope aurantia* being almost identical. In comparison,

the *Latrodectus hesperus* spectrum has a higher intensity in the 1.2 $Å^{-1}$ peak (region I) and sharper intensities in the 1.4 $Å^{-1}$ (region I) and 1.7 $Å^{-1}$ (region V) directions. The meridianal diffraction patterns appear nano-crystalline for all species. In contrast, the scattering pattern along the fiber axis is essentially isotropic, yielding a structure factor very similar in shape (but with a less intense first peak) to the equatorial curve in the perpendicular orientation (see supplementary figure). This is in agreement with previous x-ray studies.[9, 22] An increase in peak intensity in Q-space can generally be interpreted as increased ordering along these directions and since the most intense peak at 1.4 $Å^{-1}$ in the equatorial direction (region I) lies at the lowest Q-value, it might be expected that the atom-atom correlations associated with this peak extend to the longest distances in real space. However in figure 2(a) we show that this is not the case. Instead, it is observed that the longest range ordering is associated with the Bragg peaks at higher-Q in the meridional direction (5.4 $Å^{-1}$ region V). This can be explained because amorphous-like (first sharp diffraction) peaks below $Q<1.5$ $Å^{-1}$ generally decay rapidly with a periodicity of $2\pi/Q$ in real space.[23]

Moreover, based on the structure factors shown in figure 2(a), we argue that the distinction between amorphous and crystalline components is wholly ill-defined in the case of spider silks. Small well defined crystallites within a broad amorphous matrix would appear as sharp peaks upon the undulating diffuse scatter.[24] Even the most sophisticated models based on crystallites embedded in a continuous matrix fail to reproduce the high-Q diffuse scattering.[25] This indicates that the structure is dominated

by a distribution of orientated nano-crystalline and amorphous entities (or non-periodic lattice elements as proposed by B. Thiel *et al*.[26, 27]).

To determine the extent of ordering in different species of spider silks, the D(r) functions were truncated at a maximum distance of R_{max}, and Fourier transformed back into reciprocal space. This procedure was repeated as R_{max} was systematically reduced to shorter and shorter distances until the reduced χ^2-squared fit in reciprocal space exceeded a standard deviation of 5% (σ=0.05) when compared to the original S(Q) data over the range S(0.4<Q(Å^{-1})<8).[30] Using these criteria, we were able to determine the extent of the atom-atom correlations in real space, which were able to account for 95% of the measured spectra. This Q-range was chosen since it contained the sharpest peaks in the measured diffraction patterns and avoided the influence of degrading statistical noise at higher Q-values. The small differences between the transform of the truncated radial distribution function and the measured diffraction pattern manifests itself as a slight reduction in the height of the sharpest peak and a smoothing of the data throughout Q-space (see supplementary figure).

The D(r) functions comprise of several overlapping correlations making a comprehensive structural analysis difficult, but they do characterize the average local and medium range (predominantly) amorphous structure in real space. For the fibers orientated perpendicular to the x-ray beam the results are similar for all species, showing that the majority (95%) of the equatorial spectra, can be accounted for by atom-atom correlations extending out to R_{max}=7.3 Å, using the analysis described above. The

extended oscillations between 15.9 > r (Å) > 8.2 (which occur between σ=0.02 and σ=0.05) in the meridian direction are found to have only a small contribution to the corresponding S(Q), see figure 3(b). Analysis of the narrower wedge regions I to V encompass specific sharp diffraction spots and allow investigation of specific Bragg peaks in the pair distribution function. For region V, correlations are observed out to at least 20 Å in this fiber orientation. In contrast, the isotropic nature of the scattering data taken along the fiber axis yields an R_{max} of 9.1 Å for σ=0.05. Along the beam axis the equatorial and meridian D(r) curves were found to be identical and so the data were summed and the averages are shown in figure 3. The same analysis on the x-ray structure factor of glassy SiO_2 yields a value of R_{max}= 8.8 Å for σ=0.05.[28]

Although the curves for all the species give qualitatively similar results, there are some variations. In the perpedicular orientation, there is a small variation in intensity around 6 Å with the *Argiope aurantia* D(r) lying in between the other two. In the parallel orientation, *Nephila clavipes* and *Latrodectus hesperus* D(r)'s are very similar, while the *Argiope aurantia* showing slightly more intense low-r peaks. At higher distances, a small peak appears at 10.4 Å in the *Argiope aurantia* spectra compared to 9.6 Å in the *Nephila clavipes* and *Latrodectus hesperus* spectra. Here, it maybe of importance to note that *Latrodectus hesperus* and *Nephila clavipes* are rich in major ampullate spidroin 1 (MaSp1)[31] protein, which is expected to promote β-sheet formation, while *Arigopes aurantia* is rich in major ampullate spidroin 2 (MaSp2)[32] protein, which may drive more turn-like conformations.[33] The MaSp1-MaSp2 have its' largest structural influence along

the fiber axis. Nonetheless, structural differences in the real space medium range order distribution functions between species are subtle.

The first four peak positions in the D(r) functions define the average local molecular orientations in the silk and occur at distances of around 1.3 Å, 2.4 Å, 3.7 Å and 4.8 Å. The intensities of second and third peaks differ significantly in figure 3 and are most pronounced in the meridianol curve with the silk orientated perpendicular to the beam. For all the species studied here, the position, shape and intensities of the first four peaks in D(r) measured along the fiber axis, are well reproduced by the atom-atom correlations associated with the equatorial wedges (more specifically regions I , II and II) measured with the fiber perpendicular to the beam. In addition, it is important to note that the extended ordered structure in real space associated with the peaks in regions IV and V contribute very little to the molecular arrangements found along the fiber axis. This suggests that on average there is a broader distribution of local molecular orientations of fragments of sheets/chains along the fiber axis, which may be associated with the greater flexibility of the silks in this direction. Consequently, it is anticipated that the pair distribution function results presented here will provide a rigorous basis for developing a more realistic atomic scale molecular model of the amorphous part of the fiber structure than is currently available. The pair distribution function analysis presented here could also be applied to future investigations on the effects of fiber stretching and wetting on the atomic to nanometer lengthscales.

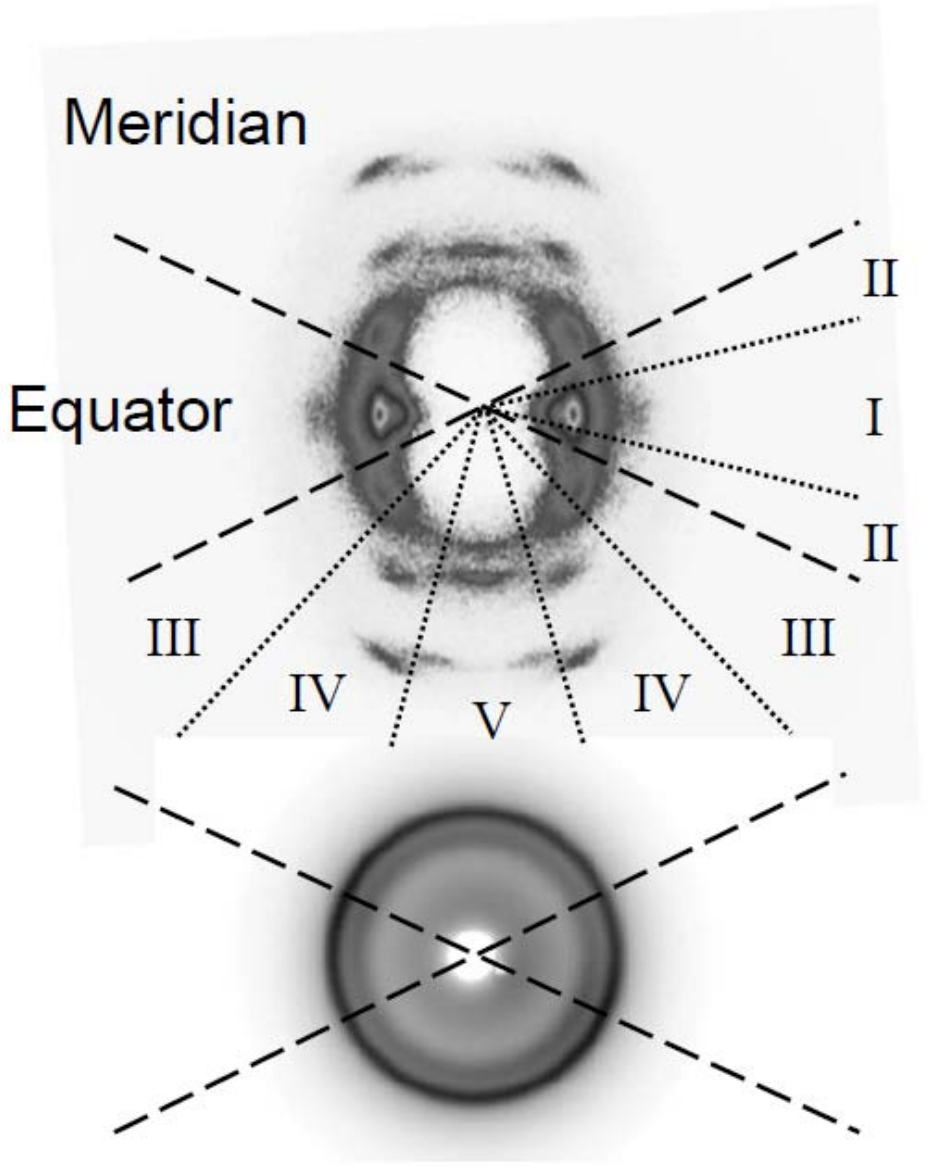

Figure 1. 2D x-ray scattering images of a *Nephila Clavipes* spider silk orientated perpendicular to the incoming beam (top) and along the fiber axis (bottom). The long dashed lines represent the equatorial and meridional wedges used to compare the silks from different species. The short dashed lines represent narrower wedges taken to investigate the influence of individual Bragg peaks in *Nephila Clavipes*; comprising of regions I and II in the equatorial plane and regions III, IV and V in the meridional plane.

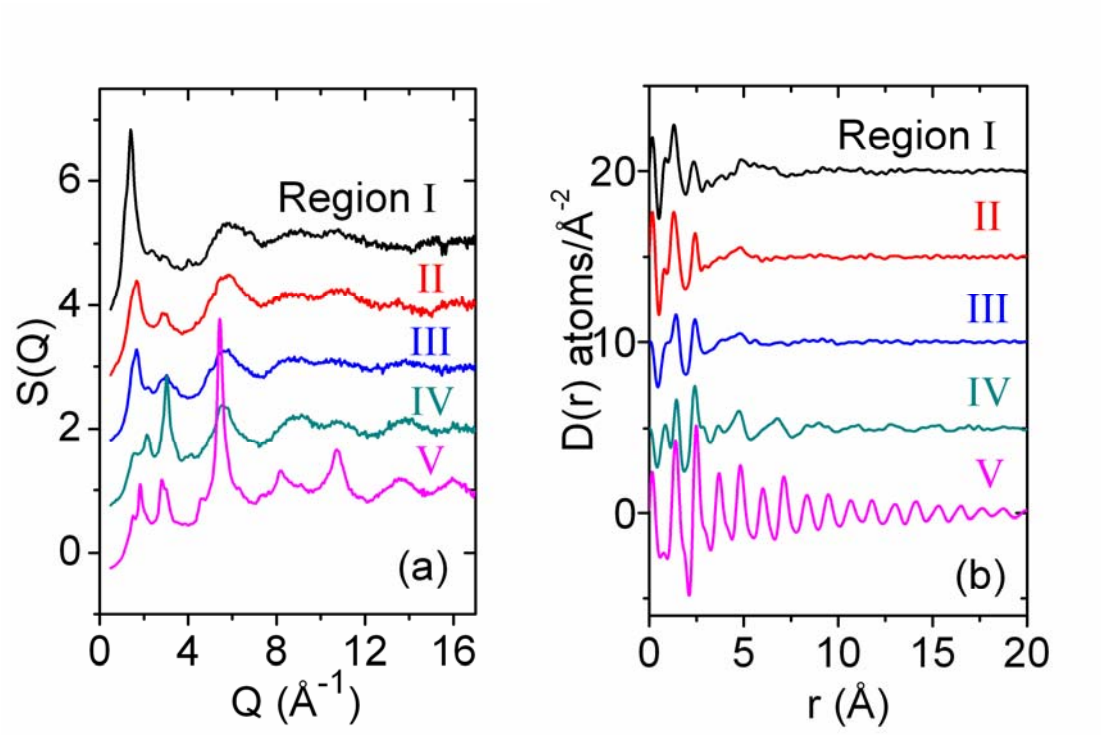

Figure 2. (a) X-ray structure factors for *Nephila Clavipes* spider silks integrated over regions I to V as illustrated in figure 1. The error bars are within the scatter of the points. (b) The corresponding atom-atom differential pair distribution functions, D(r), for regions I to V obtained using independent atom x-ray form factors. There curves were obtained by Fourier transform using a Lorch modification function using a Q_{max} of 17 Å^{-1}.[34] All curves are offset for clarity.

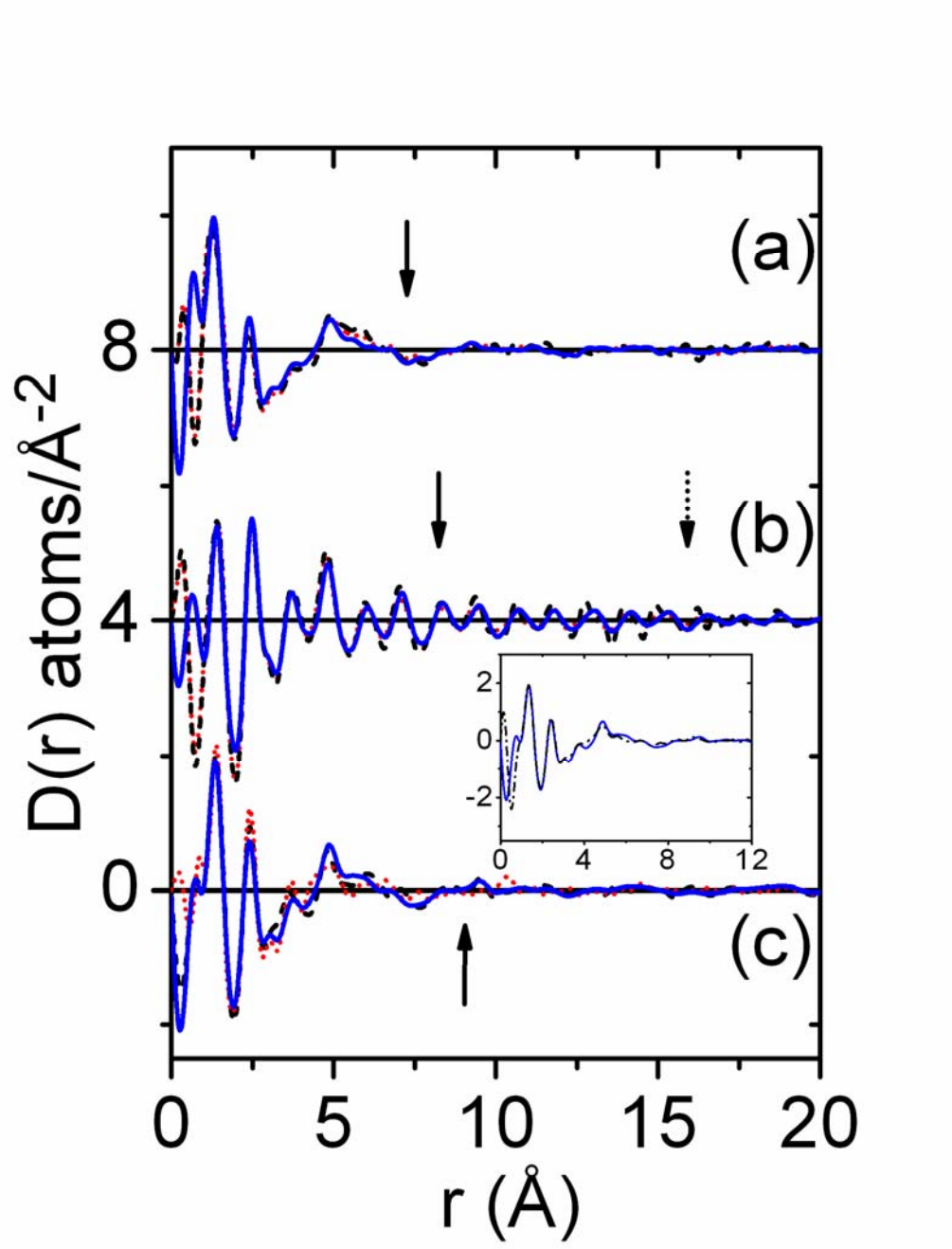

Figure 3. Differential distribution functions, D(r), for *Nephila clavipes* (solid line), *Argiope aurantia* (dotted line) and *Latrodectus hesperus* (dashed line) measured with the silk fibers orientated perpendicular to the x-ray beam for the (a) equatorial and (b) meridian wedges. (c) Represents the D(r) measured with the silk fibers orientated along axis of the x-ray beam. The curves (which are offset for clarity) were obtained by Fourier transform using a Lorch modification function with a Q_{max} of 14.2 $Å^{-1}$.[34] The value of σ=0.05 (solid arrows) and σ=0.02 (dotted arrow) are given for *Nephila clavipes* as described in the text. The insert shows (c) (solid blue line) compared to the sum of regions I,III and III (black dashed line) for *Nephila clavipes*.

Acknowledgements.
Brian Toby is thanked for useful discussions regarding the Scherrer equation. The U.S. DOE, Argonne National Laboratory under contract number DE-AC02-06CH11357 and DOE-EPSCoR under contract number DE-SC0004791 supported this work. Prof. J. L. Yarger would like to acknowledge spider silk research support from the Department of Defense, AFOSR (FA9550-10-1-0275) and the US National Science Foundation (DMR-0805197 and CHE-1011937). Also, we would like to acknowledge x-ray diffraction support from NNSA CDAC under Grant No DE-FC52-08NA28554.

References.

1. L. Eisoldt, A. Smith and T. Scheibel, Materials Today **14** (3), 80-86 (2011).
2. L. Romer and T. Scheibel, Prion **2** (4), 154-161 (2008).
3. R. V. Lewis, Chem. Rev. **106** (9), 3762-3774 (2006).
4. F. Vollrath, Reviews in Molecular Biotechnology **74** (2), 67-83 (2000).
5. Y. Termonia, Macromolecules **27** (25), 7378-7381 (1994).
6. D. T. Grubb and L. W. Jelinski, Macromolecules **30** (10), 2860-2867 (1997).
7. P. Scherrer, Nachr. Königl. Gesell. Wiss. Göttingen **26**, 98 (1918).
8. N. Du, X. Y. Liu, J. Narayanan, L. Li, M. L. M. Lim and D. Li, Biophys. J. **91**, 4528-4535 (2006).
9. C. Riekel, M. M√°ller and F. Vollrath, Macromolecules **32** (13), 4464-4466 (1999).
10. C. Riekel, C. Br‰nden, C. Craig, C. Ferrero, F. Heidelbach and M. M¸ller, International Journal of Biological Macromolecules **24** (2-3), 179-186 (1999).
11. W. Ruland, Acta Crystallographica **14** (11), 1180-1185 (1961).
12. L. Drummy, B. L. Farmer and R. Naik, Soft Matter **3**, 877-882 (2007).
13. T. Proffen and H. Kim, Journal of Materials Chemistry **19** (29), 5078-5088 (2009).
14. C. A. Tulk, R. Hart, D. D. Klug, C. J. Benmore and J. Neuefeind, Physical Review Letters **97**, 115503 (2006).
15. T. Proffen, B. S. and T. B., Zeitschrift fur Kristallographie **219** (3), III-IV (2004).
16. S. J. L. Billinge and I. Levin, Science **316** (5824), 561-565 (2007).
17. T. Proffen, S. Billinge, T. Egami and D. Louca, Zeitschrift fur Kristallographie **218** (2), 132-143 (2003).
18. J. Neuefeind and H. F. Poulsen, Physica Scripta **T57**, 112-116 (1995).
19. A. P. Hammersley, S. O. Svensson, M. Hanfland, A. N. Fitch and D. Hausermann, High Pressure Research **14** (4-6), 235-248 (1996).
20. X. Qiu, J. W. Thompson and S. Billinge, J. Appl. Crystal. **37** (4), 678 (2004).
21. J. E. Jenkins, M. S. Creager, R. V. Lewis, G. P. Holland and J. L. Yarger, Biomacromolecules **11**, 192-200 (2010).
22. C. Riekel, B. Madsen, D. Knight and F. Vollrath, Biomacromolecules **1** (4), 622-626 (2000).
23. P. S. Salmon, R. A. Martin, P. E. Mason and G. J. Cuello, Nature **435**, 75-78 (2005).
24. B. L. Thiel, K. Guess and C. Viney, Biopolymers **41** (7), 703-719 (1997).

25. S. Ulrich, A. Glišović, T. Salditt and A. Zippelius, Eur. Phys. J. E **27**, 229-242 (2008).
26. B. Thiel, D. Kunkel and C. Viney, Biopolymers **34** (8), 1089-1097 (1994).
27. B. Thiel and C. Viney, MRS Bull. **20**, 52-56 (1995).
28. Q. Mei, C. J. Benmore and J. K. R. Weber, Physical Review Letters **98** (5), 057802 (2007).
29. D. A. Keen, J. Appl. Crystal. **34**, 172-177 (2001).
30. B. H. Toby, Powder Diffraction **21** (1), 67-70 (2006).
31. M. Xu and R. Lewis, Proc. Natl. Acad. Sci. U.S.A. **87**, 7120-7124 (1990).
32. M. Hinman and R. V. Lewis, J. Biol. Chem. **267** (27), 19320-19324 (1992).
33. J. E. Jenkins, M. Creager, E. Butler, R. V. Lewis, J. L. Yarger and G. P. Holland, Chem. Comm. **46** (36), 6714-6716 (2010).
34. E. Lorch, J. Phys. C - Sol. St. Phys. **2** (2), 229 (1969).